Predicting Membrane Temperature of Condensation Free Radiant Cooling Panels

Denon Sheppard[1], Adam Rysanek[1]
[1]University of British Columbia, Vancouver, Canada

Abstract

A novel radiant cooling technology is under development that allows the panel's chilled surface to operate below the dew point of the surrounding air without condensing air moisture. This is achieved by separating the chilled surface from the humid air using a thin infrared-transparent membrane. This paper outlines the development of a generic steady-state heat transfer model used in the parametric design of future panel applications. The model is calibrated against experimental data gathered in Singapore and can accurately predict the temperature of the membrane with an average offset of $\pm 0.3°C$ from the true membrane temperature under different operating conditions. Membrane temperature of such a radiant cooling system is one of the most critical predictive outputs of such a panel's heat transfer model as panel temperature must be controlled in order to mitigate condensation risks.

Introduction

As the impacts of climate change become increasingly apparent, there is an urgent need to develop technologies that will significantly lower the energy consumption of our most significant energy end-use sectors. In many developed countries, buildings are the largest sector, accounting for 40%, 39%, and 37% of total Primary Energy Requirement (PER) in the USA, UK, and the EU respectively (Yang et al. (2014)). As the global average temperature increases, under some of the worst scenarios, global annual space heating energy demand would be set to decrease by 34%, yet cooling demand would increase by up to 72% (Isaac and van Vuuren (2009)). Focusing on efficient space-cooling technologies is of the utmost importance to combat future energy demands.

Radiant cooling has been suggested as a more efficient solution to space cooling as it: i) directs sensible cooling directly to occupants rather than cooling large volumes air that must be convected over occupants, ii) it allows for large heat pump temperature setbacks (Meggers et al. (2017)). Radiant cooling is also amenable to mixed-mode cooling applications, which leverage natural ventilation as much as possible to alleviate space cooling requirements. Prior research has shown that the potential energy savings of radiant cooling systems over conventional air-conditioning vary widely, from 7 to 85%, attributed to the favourability of different climates (Feng (2014)). Savings are found to be low in mild, humid climates, and potentially high in hot, dry climates. The challenge of proposing radiant cooling systems in hot and humid climates remains that, whilst these climates do face high sensible cooling loads and would benefit theoretically from radiant cooling, the high dew point of these environments make traditional radiant cooling systems infeasible without additional use of a dehumidification (or latent cooling) system. In these situations, the savings afforded by radiant cooling are subsumed by the added cost and energy of a parallel latent cooling system.

A novel radiant cooling technology has recently been developed and demonstrated to provide sensible cooling in hot and humid climates without the need for additional latent cooling. The technology, inspired by an idea first conceived by Morse (1963), and experimented on at Princeton University (Teitelbaum et al. (2019)) more than 55 years later, was tested at an operational-scale in the form of an outdoor radiant cooling pavilion designed, constructed, and evaluated in Singapore over 2018-2019, shown in Figure 1 (Teitelbaum et al. (2019)).

The pavilion operated by surrounding human participants with 10 radiant cooling panels. Each panel operated as follows. A chilled surface, cooled by water, was separated from the ambient environment by placing it in an insulated, and desiccated rectangular casing that is sealed air-tight by an infrared-transparent membrane. A provisional cross-section of this panel is shown in Figure 2. The panel allows the chilled radiating surface to be kept well-below the dew point of the ambient air, while still avoiding condensation on the membrane itself. The spacing of the membrane from the chilled surface is designed so that the equilibrium temperature of the membrane is sufficiently above ambient dew point temperature across all potential operational conditions (Teitelbaum et al. (2019)). Increasing the distance between the chilled

Figure 1: The Cold Tube pavilion constructed using 10 condensation free radiant cooling panels (Teitelbaum et al. (2019)).

surface and the humid air will increase the operating temperature of the membrane, and so the panel can be designed for different climates to ensure that the membrane temperature is never lower then the dew point of the surrounding air. The membrane, made of polyethylene, is transparent to 80% of the thermal radiation exchange between the chilled surface and human bodies engaged with it (Teitelbaum et al. (2020)). The radiation absorbed by the membrane (20% of incident infrared radiation) introduces a potential system inefficiency at present, but it is possible that future materials may be produced that provide higher transmissivity in the mid-range infrared spectrum needed for such applications.

This paper looks to move this novel radiant cooling technology closer to widespread implementation by developing and calibrating a steady-state parametric model that can predict the membrane temperature of the panel under different operating and environmental conditions. The underlying physics of the model is presented in the following sections. The model is calibrated using experimental data collected in Singapore. Calibration parameters are selected using the Morris method, and calibration of these parameters is undertaken by applying a Monte Carlo search of optimum parameter values. While the panel can be installed in both the vertical and horizontal orientation (as seen in Figure 1), this study will focus on a vertical panel because experimental data needed for model validation was not obtained for a horizontal panel.

Methods

Model Creation & Modes of Heat Transfer

At the core of the heat transfer model exists an energy balance centered on the infrared-transparent membrane. As there is no known, commercially-available and/or affordable temperature sensor (such as a thermistor or thermocouple) that is transparent to infrared radiation similar to polyethylene, it is not possible to readily measure membrane temperature in operational settings. Any conventional surface temperature sensor would interact radiatively with surrounding surfaces in an order of magnitude greater than the membrane itself.

The heat transfer model being developed for a vertical panel allows for the determination and control of the membrane temperature without it being measured during operation. By computing the heat transfer model using spectral transmissivity data, the radiant flux that the panel can provide to occupants can be simultaneously estimated. Although similar in principle, the heat transfer model for a horizontal panel can not be created at present as there is currently no experimental data available for model verification.

Equation 1 models the steady state membrane temperature, and each mode of heat transfer, Q_{1-5}, is explained further in the following subsections. Q_{1-3} are the three sources of radiant heat transfer, and Q_{4-5} are internal and external natural convection. The model is coded in Python and is intended to be solved numerically, calculating Equation 1 using a range of membrane temperatures and recording the results. The membrane temperature that results in the left side of Equation 1 being closest to 0 is used as the model's membrane temperature prediction. The membrane temperatures tested in the model are evenly spaced between the chilled surface and highest environmental temperature (radiant temperature or air), and the number of temperatures considered can be increased to improve model precision but will also increase computation time.

$$Q_1(T_M) + Q_2(T_M) + Q_3(T_M) + Q_4(T_M) + Q_5(T_M) = 0 \quad (1)$$

T_M : Membrane temperature

The 5 modes of heat transfer are shown in Figure 2. All surfaces emit radiant heat, so the energy emitted by each surface is analyzed separately to determine how it affects the membrane. Additionally, two forms of natural convection take place. External natural convection transfers heat from the air surrounding the panel to the membrane, while internal natural convection transfers heat from the membrane to the chilled surface.

Convective Heat Transfer, Q_{4-5}

In any radiant cooling application, the chilled surface of the proposed panel will be operating at a surface temperature lower than the environment's air temperature. This means that the membrane will always be at a temperature between the temperatures of the chilled surface and the surrounding air, and heat will travel convectively from the surrounding air to the membrane, and from the membrane, through the panel's internal dry air, to the chilled surface. The convection happening within the panel (Q_4) is natural, while the convection external to the panel (Q_5) is likely a mix of natural and forced convection (mixed convection) (Teitelbaum et al. (2020)).

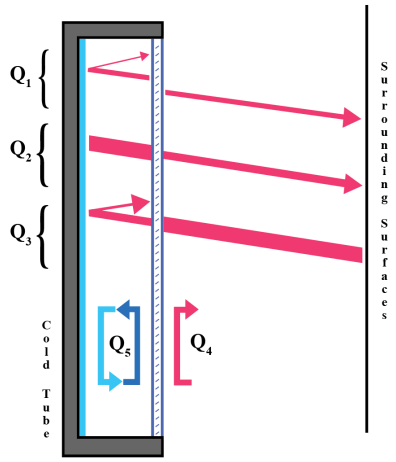

Q_1: Radiation Emitted by the Membrane
Q_2: Radiation Emitted by the Chilled Surface
Q_3: Radiation Emitted by the Participating Surfaces
Q_4: External Natural Convection
Q_5: Internal Natural Convection

Figure 2: The modes of heat transfer affecting the membrane.

For both free, forced, and mixed convection, the total heat being transferred between a solid and a fluid at steady-state is estimated using Equation 2.

$$Q_{conv} = hA(T_f - T_M) \tag{2}$$

h : convective heat transfer coefficient
A : surface area
T_M : surface temperature of membrane
T_f : temperature of fluid

A and T_f are readily available, and T_M is the membrane temperature which is iterated using the numerical model. Q_{conv} can't be determined in isolation as it depends on the other modes of heat transfer in Equation 1, so another equation must be used to determine h.

To derive h for the internal and external flow scenarios, the Nusselt number (Nu), for said scenarios must be estimated. The Nusselt number represents the ratio of convective to conductive heat transfer that is occurring at the solid-fluid interface. This relationship can be seen in Equation 3.

$$Nu_L = \frac{\text{convective heat transfer}}{\text{conductive heat transfer}} = \frac{hL}{k} \tag{3}$$

L : characteristic length of flow scenario
k : conductivity of air

Thermal conductivity of air (k) can be determined using the known air temperatures; L varies depending on the scenario, but is readily available. Nu is still unknown which prevents the estimation of h, and in turn the estimation of Q_{conv} in Equation 2. Fortunately, many empirical correlation have been developed for different heat transfer scenarios that allow for the estimation of Nu using geometry and air properties (Ghiaasiaan (2011)).

The empirical correlation for determining Nu changes depending on the convection scenario. Q_4 and Q_5 are both derived from Q_{conv}, and represent the internal and external convective heat transfer modes that are affecting the membrane, each requiring a different Nu correlation. The Prandtl number (Pr) is present in most Nusselt number correlations, and is estimated using known air properties.

Internal Natural Convection

All Nusselt number correlations are taken from Ghiaasiaan (2011), and air properties were estimated using CoolProp (Bell et al. (2014)). For natural convection in a vertical panel, two correlations are used that change depending on the flow's Rayleigh number (Ra). The model uses Equation 4 when Ra is less than 10^7 and Equation 5 when it is greater.

$$\text{For: } 10 < \frac{l}{S} < 40, 1 < Pr < 2(10^4), 10^4 < Ra_S < 10^7$$

$$Nu_s = 0.42 Ra_s^{0.25} Pr^{0.012} (\frac{l}{S}) \tag{4}$$

$$\text{For: } 10 < \frac{l}{S} < 40, 1 < Pr < 20, 10^6 < Ra_S < 10^9$$

$$Nu_s = 0.046 Ra_s^{0.33} \tag{5}$$

Using the appropriate Nusselt number correlation in Equation 3, Q_4 can be estimated using Equation 6.

$$Q_4 = A_M \frac{k}{l} Nu_s (T_{cs} - T_M) \tag{6}$$

As internal convection transfers thermal energy between the chilled surface (cs) and the membrane, the temperature range used to calculate total heat transfer is different then the range presented in Equation 2. The temperature of the air inside the panel is estimated as being equal to the average temperature of these two surfaces.

External Natural Convection

The method used to estimate external natural convection is similar to that of internal. The Nu equation for a vertical panel can be seen in Equation 7.

$$\langle Nu_l \rangle_l = \{0.825 + \frac{0.387 Ra_l^{\frac{1}{6}}}{[1 + (0.492/Pr)^{\frac{9}{16}}]^{\frac{8}{27}}}\}^2 \tag{7}$$

External Forced Convection

As the panel is outdoors, where it is possible for airspeed to be predicted from weather data or locally measured, as it was within the Singapore pavilion,

the Reynolds number (Re) for flow in a forced convection regime can be estimated. This Re is used to estimate the Nusselt number correlation for a low velocity laminar flow parallel to a flat plate, shown in Equation 8.

$$\langle Nu_l \rangle_l = 0.664 Pr^{1/3} Re_l^{1/2} \tag{8}$$

When the effects of both forced and natural convection are relevant, the Nusselt numbers for both flows are combined using Equation 9 to find the mixed convection Nusselt number.

$$Nu_{mixed}^n = Nu_F^n \pm Nu_N^n \tag{9}$$

Nu_F : forced convection Nusselt number
Nu_N : natural convection Nusselt number

n is equal to 3 as seen in Ghiaasiaan (2011) and the two Nusselt numbers are added as buoyancy forces work with the wind to increase convection. Now that the mixed convection Nu number is estimated, it can be used to estimate Q_5 as seen in equation 10.

$$Q_5 = A_M \frac{k}{l} Nu_{mixed}(T_{air} - T_M) \tag{10}$$

Radiant Heat Transfer, Q_{1-3}

Radiant heat is emitted from all materials that are at a temperature above 0K. As the energy balance is centered on the membrane, energy is removed from the balance only when the membrane emits thermal energy, and energy is added when the membrane absorbed thermal energy from any source. There are 3 surfaces that interact radiantly with the membrane. From Equation 1, Q_1 is the effect that the energy emitted by the membrane has on the internal energy of the membrane. Q_2 is the effect the energy emitted by the chilled surface (cs) has on the internal energy of the membrane, and Q_3 is the effect of the surfaces surrounding the membrane (ss).

The term spectral will be used throughout this section. It means the property being discussed is being analyzed at each measured wavelength across the electromagnetic spectrum. For example, when talking about spectral irradiance, the irradiation value at each wavelength must be considered separately.

The principles of the developed model regarding radiant heat transfer comes from Incropera et al. (2007). The terms that describe radiation leaving or impinging on a surface are as follows.

$$E_\lambda : Emission$$
$$G_\lambda : Irradiance$$
$$J_\lambda : Radiosity$$

See Figure 3 to help visualize how radiation interacts with surfaces. Emission is the energy being emitted by a surface, thereby lowering its internal energy. Irradiance is the energy impinging on a surface, which can be reflected, transmitted, and/or absorbed, as seen in Equation 11 and 3(b). Radiosity is the total energy leaving a surface, which is the combination of the surface's emission and the reflected portion of the irradiance on the surface.

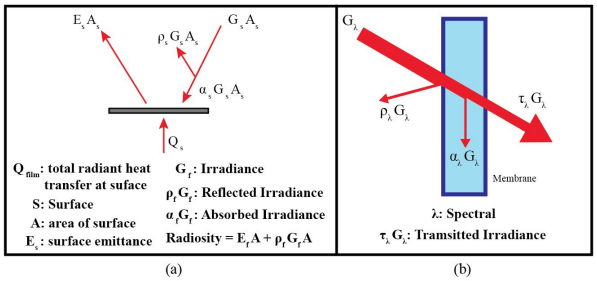

Figure 3: (a)Emission and irradiation on an opaque surface (b) Irradiation on a translucent surface

The spectral properties of the membrane were measured using an FTIR machine. This machine directly measures the membrane's spectral reflectivity and transmissivity. The membrane's absorptivity can then be estimated using Equation 11.

$$\alpha_\lambda + \tau_\lambda + \rho_\lambda = 1 \tag{11}$$

α_λ : absorptive coefficient
τ_λ : transmittance coefficient
ρ_λ : reflective coefficient

From Equation 12, emissivity can be estimated as the emissivity of a material is equal to its absorptivity.

$$\epsilon_\lambda = \alpha_\lambda \tag{12}$$

The net heat transfer at the membrane due to any emitting surface is estimated using Equation 13.

$$Q_{rad} = A_M \left[\int_{\lambda_1}^{\lambda_2} \alpha_{\lambda_M} \sum G_{\lambda_M} d\lambda - \int_{\lambda_1}^{\lambda_2} E_{\lambda_M} d\lambda \right] \tag{13}$$

Where $\int_{\lambda_1}^{\lambda_2} \alpha_{\lambda_M} \sum G_{\lambda_M} d\lambda$ is the energy absorbed by the membrane, which is equal to the total irradiation on the membrane factored by the membrane's absorptive coefficient. $\int_{\lambda_1}^{\lambda_2} E_{\lambda_M} d\lambda$ is the energy emitted by the membrane. Q_{1-3} are all derived from this equation. Q_2 and Q_3 look at energy emitted by surfaces other than the membrane, which makes the E_{λ_M} term in Equation 13 equal to zero.

When estimating Q_{rad} for any of the 3 modes of radiant heat transfer (Q_{1-3}) , first the spectral, hemispherical emissive power (E_λ) $[W/m^2/\mu m]$ emitted by the surface of interest must be estimated. This is done using Equation 14.

$$E_\lambda(\lambda, T) = \left[\frac{C_1}{\lambda^5 [exp(\frac{C_2}{\lambda T})]} \right] \epsilon_\lambda \tag{14}$$

This equation estimates the emissive power of a black body, and scales it by the known emissivity of the surface being analyzed. The spectral emissivity of the membrane is determined using FTIR data, while the chilled surface has an emissivity of 0.95. Radiant temperature measurements were used to determine the radiant energy being emitted by the surfaces surrounding the panel. This process measures the thermal power being absorbed by an array of pyrgeometers, and calculates the required temperature of the sensor's surroundings to emit this quantity of energy. By using an assumed emissivity of 1 for these surfaces, the radiant emission from these surfaces can be estimates using the surface's measured radiant temperature. An emissivity of 1 implies that no reflections occur when radiation impinges on the surrounding surfaces.

If Q_{2-3} is being estimated, the emitted radiation does not interact with anything prior to impinging on the film, thus the first source of irradiation on the film $(G_{1_{\lambda_M}})[W/m^2/\mu m]$ is estimated using equation 15.

$$\text{For } Q_{2-3}: \quad G_{1_{\lambda_M}} = E_{\lambda_{cs,\ ss}} \tag{15}$$

As discussed before, radiation does not reflect off the surrounding surfaces, so there is no second irradiation component used in the estimation of Q_2 (as seen in Figure 2).

When estimating Q_3, the irradiation estimated using Equation 15 is transmitted through the membrane. This transmitted energy then reflects off the chilled surface and returns to again impinge on the membrane, which is the second source of irradiation on the membrane $(G_{2_{\lambda_M}})$. This is estimated using Equation 16.

$$\text{For } Q_3: \quad G_{2_{\lambda_M}} = G_{1_{\lambda_M}} * \tau_{\lambda_M} * \rho_{\lambda_{cs}} \tag{16}$$

If Q_1 is being estimated, the radiation emitted from the side of the film facing the chilled surface reflects off said surface before returning to the film. When estimating Q_1, the first and only source of irradiation on the film is estimated using Equation 17.

$$\text{For } Q_1: \quad G_{1_{\lambda_M}} = E_{\lambda_M} * \rho_{\lambda_{cs}} \tag{17}$$

Equations 13 - 17 lead to the creation of Equations 18 - 20 which allow us to estimate Q_1, Q_2, and Q_3.

$$Q_1 = 2A_M \int_{\lambda_1}^{\lambda_2} \alpha_{\lambda_M} G_{1_{\lambda_M}} - E_{\lambda_M} d\lambda \tag{18}$$

$$Q_2 = A_M \int_{\lambda_1}^{\lambda_2} \alpha_{\lambda_M} G_{1_{\lambda_M}} d\lambda \tag{19}$$

$$Q_3 = A_M \int_{\lambda_1}^{\lambda_2} \alpha_{\lambda_M} (G_{1_{\lambda_M}} + G_{2_{\lambda_M}}) d\lambda \tag{20}$$

In Equation 18 the area is doubled because the membrane emits in both directions.

Conductive Heat Transfer

Conduction is not present in this energy model. It is assumed that conduction at the membrane does not affect the membrane temperature given the small surface area connecting the membrane to the panel. It is also assumed that, for the purposes of this model, the membrane is thin and conduction through it negligible.

Experimental data

To asses the performance of the model, data points were collected during the Singapore pavilion experiment in December 2018 and January 2019. The model requires four inputs, the temperature of the chilled surface, the temperature of the ambient air, the radiant temperature inside the pavilion, and the air speed inside the pavilion. The temperature of the chilled surface was determined by measuring the temperature of the chilled water entering and exiting the panel, via a capillary mat, and taking the average. The temperature of the air inside the pavilion was measured using Pt-100 thermistors (± 0.1 C) that were shielded from radiation using a highly reflective silver cone.

To measure the radiant temperature inside the pavilion, 6 pyrgeometers (Apogee, SL−510−SS; 0.12 mV per Wm−2; 1% measurement repeatability; 5% calibration uncertainty; $\pm^o$C) were arranged orthogonally on a small wooden cube. Pyrgeometers consist of a high accuracy thermistor that continuously measures the device's internal temperature and are isolated from convection and conduction. The device also creates a voltage output that is proportional to the radiant flux received from a 150 degree field of view. Knowing both the device's temperature and radiant flux, one can solve for the average radiant temperature of its surroundings.

$$q_{pyrg\ rad} = \sigma(T_{pyrg}^4 - T_{rad\ temp}^4) \tag{21}$$

Unfortunately air velocity and radiant temperature were not measured at the same time as membrane condensation. A correlation was created that estimates radiant temperature using the chilled surface temperatures present during the condensation measurements. Data sets were gathered that include chilled surface temperatures within 0.2^oC of the chilled surface temperatures present during the condensation measurements, as well as radiant temperature. Excel was used estimate an equation that best correlates the chilled surface temperatures to the radiant temperature values, as seen in Equation 22.

$$T_{rad\ temp} = 0.6766 T_{cs} + 13.557 \tag{22}$$

An average air velocity value of 0.3 m/s (see Figure

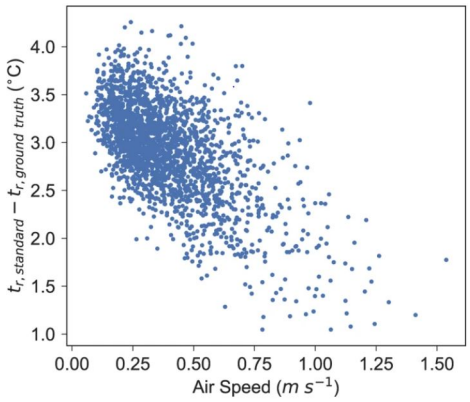

Figure 4: Wind speeds measurements inside pavilion.

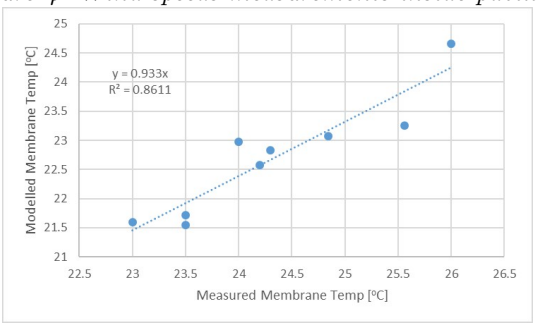

Figure 5: Correlation between modelled and measured membrane temperatures using Non-calibrated model.

4) is used in the model based on longitudinal data collected at the pavilion in and around the day of experiments.

It is difficult to measure membrane temperature directly, as a thermocouple/thermister can be affected by radiation and convection, and using a radiant temperature sensor will be affected by the temperatures of both the membrane and the chilled surface behind it. The method that was implemented was to decrease the chilled surface temperature slowly until condensation formed at the center of the panel. By measuring the relative humidity inside the pavilion (ThermCondSys 5500 measurement system), the dew point temperature can be calculated which is also the temperature of the membrane when condensation occurs.

Results

Figure 5 shows the correlation between modeled and measured membrane temperatures produced when using the non-calibrated model.

Although the model consistently under-predicts the real membrane temperature by about 1.3^{o}C, some of the model parameters, such as the Nusselt numbers for internal and external convection, are likely not sufficiently accurate as discussed in the following errors section. It is reasonable to attempt to enhance the performance of the model by scaling parameters that are uncertain. To do this, the parameters that have the greatest effect on the model output should be identified. A sensitivity analysis using the Morris method (Campolongo et al. (2007)) was conducted to accomplish this. The parameter inputs that were studied are shown in the left column of Table 1, accompanied by their respective μ^*, μ, and σ values.

Table 1: Morris Results.

Parameter	$\boldsymbol{\mu^*}$	$\boldsymbol{\mu}$	$\boldsymbol{\sigma}$
cs temp	5.006	5.006	1.836
h exterior	4.878	4.878	2.028
h interior	4.188	-4.188	1.542
outdoor air temp	3.655	3.655	1.198
ss temp	1.625	1.625	0.536
cs emissivity	0.328	-0.328	0.235

μ and σ represent the mean and variance of the parameter's elementary effects. An elementary-effects sensitivity analysis is a time efficient way to determine the importance of the model inputs. The values seen in Table 1 are qualitative, meaning that they allow for the identification of non-influential inputs, but they don't quantify the exact relative importance of each input. μ^* is the value that best reflects total sensitivity of each parameter. From the results presented, the interior and exterior convection coefficients have a relatively large impact on the output of the model, while the impact of emissivity of the cold surface is relatively small. The temperature of the cold surface appears to be the most sensitive parameter. However, this and other temperature parameters such as the outdoor air temperature are known from data and are not intrinsic model parameters. It appears from the sensitivity analysis that the convective heat transfer coefficients are the most sensitive parameters of study, and therefore the model calibration is undertaken against iterations of these two parameters.

It is logical that the source of error lies in the h coefficients as they are derived using several estimated quantities. Therefor, applying a constant error factor to the estimated h values could compensate for the errors present in the calculation. This is to say that equations 6 and 10, used to estimate Q_4 and Q_5 in equation 1, were altered by applying estimated internal and external error factors (Er_{int} and Er_{ext}) to the respective h values. The updated method for predicting Q_4 and Q_5 can be seen in equations 23 and 24.

$$Q_4 = A_M Er_{int} \frac{k}{l} Nu_s (T_{cs} - T_M) \tag{23}$$

$$Q_5 = A_M Er_{ext} \frac{k}{l} Nu_{mixed} (T_{air} - T_M) \tag{24}$$

Where $h = \frac{k}{l} Nu$ as seen in Equation 3. To estimate the error factor values, a Monte Carlo simulation with 3500 samples was conducted, where the internal and external convection coefficient error factors (Er_{int} and Er_{ext}) were randomly varied between

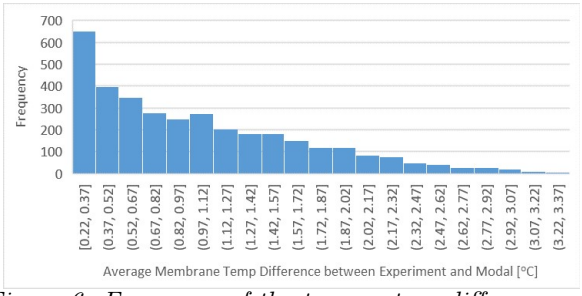

Figure 6: Frequency of the temperature difference results produced using the Monte Carlo simulation

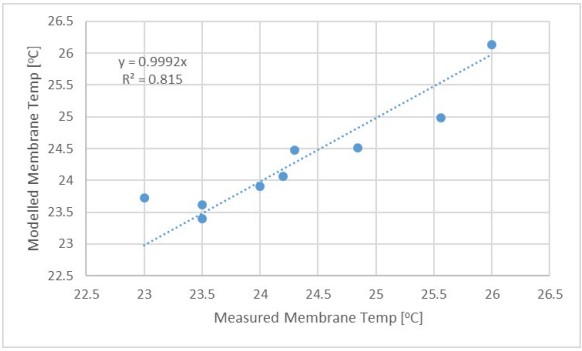

Figure 7: Correlation between modelled and measured membrane Temperatures after applying error factors.

0.01 and 2. For each of the Monte Carlo iterations, the sample for internal and external error factors were used to estimate the membrane temperature under each of the 9 measured operating condition (see Figure 5). The average difference between the model's estimated membrane temperatures and the measured membrane temperatures were recorded for each set of randomly sampled error factor values. The distribution of Er_{int} and Er_{ext} values present in the top 5% of temperature difference results (smallest temperature difference) were used to estimate the true error factor values. The histogram showing the distribution of average temperature difference results produced during the Monte Carlo simulation can be seen in Figure 6.

The mean and standard deviation of the top 5% of best performing samples can be seen in Table 2

Table 2: Error Factors.

Error Factor	Mean	Standard Deviation
External	1.11	0.28
Internal	0.41	0.24

The data would suggest that the error factor that corrects h_{ext} is approximately 1.11, and the error factor that corrects h_{int} is 0.41. These values suggests that the external convection coefficient is modeled reasonably accurately, while there are significant errors present in the modeling of the internal convection coefficient.

Figure 7 shows the correlation between modeled and measured membrane temperatures when using these values. The calibrated energy model can accurately predict the film temperature under different operating conditions with an average error of $\pm$ 0.27^{o}C.

Discussion

Sources of model Errors

The first error source is in the estimation of the internal natural convection Nusselt numbers. Equations 4 and 5 are used but Ghiaasiaan (2011) puts forth 4 equations that apply to vertical-rectangular enclosures. These two were used because their parameter ranges are closest to the experimental panel in Singapore and they produced the best results when all 4 were tested. That being said, the parameter ranges do not perfectly apply to the tested panel. The Pr value of the air is approximately 0.7. While the bottom of the Pr range for both equations is 1.

The Nu correlations were developed in labs and it's hard to know if the experiments that were conducted to derive them accurately reflect this experimental setup. For instance, even though the height to depth ($\frac{l}{S}$) ratio of the panel falls within the low range for both correlations, these Nu correlation experiments were likely conducted in an enclosure of a much smaller size. It is possible that fluid flows arise in a large panel that are not present during the experiments, and would therefor decrease the compatibility of equations. This argument also applies to the external Nu correlation used.

The model uses spectral membrane transmissivity values that are equal to the FTIR transmissivity measurements conducted on the membrane used in Singapore. There are several reasons why this assumption is poor, as radiation could be obstructed due to dirt/imperfections on the film, and sections of the film could be sagging which would change the way radiation refracts during transmission. The model's sensitivity to membrane transmissivity should have been included in the Morris sensitivity analysis.

Table 1 shows that the model is highly sensitive to the temperature of the cold surface. As seen in Figure 1, the capillary mat is the primary surface interacting radiantly with the occupant, so the average of the input and output temperatures in the capillary mat should provide a reasonably accurate average surface temperature. However, the high sensitivity means that this assumption should be further investigated through experimentation.

Finally, radiant temperature and wind speeds were not recorded during the membrane temperature measurements. A regression was made to correlate measured radiant temperature with chilled surface temperatures using separate data but this is not an ideal approach. Model wind speeds were assumed to be 0.3 m/s as this was the most frequently measured value.

Future Work

It has been shown that the membrane temperature can be predicted with an average accuracy of $\pm$0.27°C, at least for the range of experimental data encountered in Singapore. However, only the sensi-

tivity of high level model parameters are known. To improve the applicability of the model to different operating/environmental conditions, a further sensitivity analysis should be conducted that looks at the base level inputs of the model to increase the precision of the calibration approach. This will provide a deeper understanding of the model and will identify which model parameters need to be confirmed. The model's sensitivity to the film membrane will also be included.

More membrane temperature data points need to be collected and used to further calibrate the model. The data points available span a wide range of operating conditions and the model can accurately predict them. However the small sample size currently available will likely cause skepticism. Additionally, radiant temperature and wind speeds need to be measured during these measurements to remove the previously mentioned source of error.

Equations will be implemented that allow for the modeling of the transient response of the panel to its environment. This was not included because transient membrane temperature data was not available for calibration.

Finally, membrane temperature measurements need to be conducted on a radiant cooling panel operating in a horizontal orientation so that this panel orientation can be added to the model and calibrated.

Conclusions

This study confirms that the membrane temperature of a novel condensation free radiant cooling panel can be predicted within an appropriate degree of accuracy. However, errors are present in some aspect of the model's construction that have required the creation of internal and external convection coefficient error factors via a Morris sensitivity analysis and a Monte Carlo optimization. These factors were applied to the estimated internal and external convective heat transfer coefficients and significantly increase the performance of the model.

As it stands, the model predicts the temperature of the membrane with an average offset of $\pm 0.27^{o}$C. A deeper sensitivity analysis must be conducted to further develop the model.

References

Bell, I. H., J. Wronski, S. Quoilin, and V. Lemort (2014, February). Pure and Pseudo-pure Fluid Thermophysical Property Evaluation and the Open-Source Thermophysical Property Library CoolProp. *Industrial & Engineering Chemistry Research 53*(6), 2498–2508. Publisher: American Chemical Society.

Campolongo, F., J. Cariboni, and A. Saltelli (2007, October). An effective screening design for sensitivity analysis of large models. *Environmental Modelling & Software 22*(10), 1509–1518.

Feng, J. D. (2014, April). Design and Control of Hydronic Radiant Cooling Systems.

Ghiaasiaan, S. M. (2011). Cambridge University Press.

Incropera, F. P., A. S. Lavine, T. L. Bergman, and D. P. DeWitt (2007). *Fundamentals of heat and mass transfer*. Wiley.

Isaac, M. and D. P. van Vuuren (2009, February). Modeling global residential sector energy demand for heating and air conditioning in the context of climate change. *Energy Policy 37*(2), 507–521.

Meggers, F., H. Guo, E. Teitelbaum, G. Aschwanden, J. Read, N. Houchois, J. Pantelic, and E. Calabrò (2017, December). The Thermoheliodome – "Air conditioning" without conditioning the air, using radiant cooling and indirect evaporation. *Energy and Buildings 157*, 11–19.

Morse, R. (1963). Radiant cooling. *Architectural Science Review 6*(2), 50–53.

Teitelbaum, E., K. W. Chen, F. Meggers, H. Guo, N. Houchois, J. Pantelic, and A. Rysanek (2020, February). Globe thermometer free convection error potentials. *Scientific Reports 10*(1), 1–13. Number: 1 Publisher: Nature Publishing Group.

Teitelbaum, E., K. W. Chen, F. Meggers, J. Pantelic, D. Aviv, and A. Rysanek (2019, nov). The cold tube: Membrane assisted radiant cooling for condensation-free outdoor comfort in the tropics. *Journal of Physics: Conference Series 1343*, 012080.

Teitelbaum, E., A. Rysanek, J. Pantelic, D. Aviv, S. Obelz, A. Buff, Y. Luo, D. Sheppard, and F. Meggers (2019, March). Revisiting radiant cooling: condensation-free heat rejection using infrared-transparent enclosures of chilled panels. *Architectural Science Review 62*(2), 152–159.

Yang, L., H. Yan, and J. C. Lam (2014, February). Thermal comfort and building energy consumption implications – A review. *Applied Energy 115*, 164–173.